Optical diffractions as probes to surface diffusion of adsorbates

X. D. Zhu
Department of Physics, University of California, Davis, CA 95616-8677

ABSTRACT

I review some of the general aspects of using optical diffractions from laser-induced surface density gratings to probe diffusion of adsorbates. Among examples, the recent progress in the study of quantum tunneling diffusions is emphasized.

1. INTRODUCTION

Diffusion of adsorbates on a surface is one of the fundamental steps in gas-solid interaction dynamics. A comprehensive understanding of surface diffusion is a prerequisite for understanding many surface dynamical processes such as catalytic reactions, epitaxial crystal growth, corrosion, and material processing.[1] Fundamentally, a moving particle on a surface is a sensitive probe to surface morphology. More recently, it has been demonstrated by Gomer and coworkers that the diffusion of light atoms on surfaces represents an important test case other than the diffusion of muons in solids for investigations of quantum tunneling.[2–12] The weaker surface potential modulation on a solid than its bulk counterpart leads to a larger delocalization of the wave functions of light adatoms and therefore an earlier onset of quantum tunneling diffusion.[14,15]

Recently, we and a number of other groups have successfully explored optical diffractions from monolayer density gratings of adsorbates as probes to surface diffusions.[16–21] The density gratings are created by laser-induced desorption with a pair of interfering laser pulses.[22,23] As the diffusive motion of remaining adsorbates tends to smear out the density modulation, the change of optical diffraction signals from the gratings is used to deduce surface diffusion coefficients. Both linear and second-harmonic diffractions have been successfully employed to measure surface diffusion of adsorbates. This effort has been fueled by the attractive features of an optical diffraction technique: (a) it can measure diffusion coefficients from 10^{-7} cm^2/sec to 10^{-16} cm^2/sec; (b) it is capable of probing the anisotropy of a diffusion with extremely high aspect ratios; (c) it is sensitive to density modulations of 2% of one monolayer; (d) it is non-evasive to surface diffusion processes. In this paper, I will briefly review some of the general aspects of the experimental consideration and the analysis of an optical diffraction technique. More details may be found in the published literatures.[16–24] As examples, I will describe briefly the experimental results of the diffusion of CO on Ni(111) and Ni(110), and hydrogen and deuterium on Ni(100) and Ni(111).[25]

2. GENERATION OF MONOLAYER DENSITY GRATINGS BY LASER-INDUCED DESORPTION WITH INTERFERING OPTICAL FIELDS:

Laser-induced gratings have long been exploited in studies of transient properties of material excitations including relaxation and transport in both gaseous and condensed media.[26] The laser-based techniques promise highest time-resolution ($< 10^{-13}$ sec) and highest spectral resolution for species selective excitation. The high aspect ratios of laser beam diameters to laser-induced grating spacings are ideal for studies of transport processes with anisotropy. It seems natural that laser-induced grating techniques should be applicable to surface transport measurements. For the purpose of a surface diffusion measurement, laser-induced gratings present an appropriate length scale for the observation of the quantum tunneling effect.[19,21]

Adsorbate density gratings can be produced through either resonant photo-desorption or thermal desorption effect.[22,23] I will describe the thermal desorption method here.

A typical experimental arrangement is shown in Fig. 1. A single crystal substrate is placed in an ultrahigh vacuum chamber. It exposes a low Miller index plane (e.g., [100], [110], and [111]) of interest. The surface is usually cleaned through cycles of ion sputtering, annealing and oxidation in vacuo. The cleanliness is verified and

 0-8194-1083-7/93/$6.00

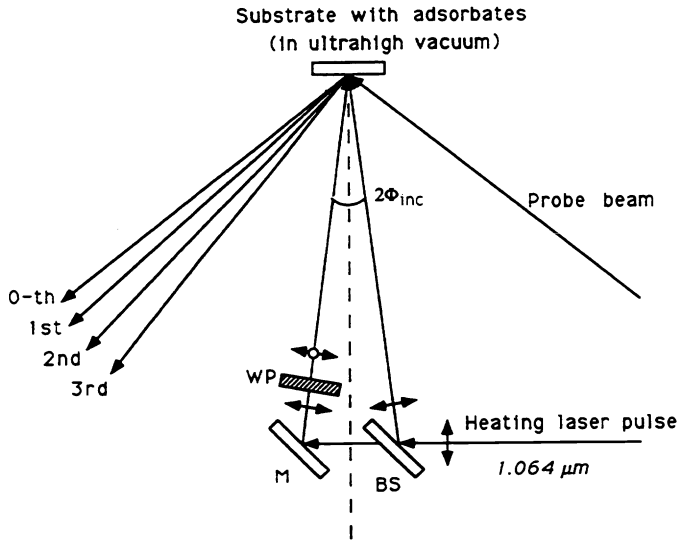

Fig.1. Sketch of an experimental arrangement for the generation and detection of monolayer adsorbate density gratings with lasers. For surface diffusion measurements on single crystal substrates, the samples are placed in ultrahigh vacuum chambers. M is a dielectric mirror. BS is a beam splitter. WP is a half-wave plate which can change the linear polarization of the heating laser pulse from a p-wave (indicated by double arrows) to a s-wave (indicated by an open circle) continuously.

characterized by Auger electron spectrometry. The substrate is then cooled to a measurement temperature at which adsorbates are allowed to cover the surface through gas phase deposition. By adjusting the dosage (in unit of Langmuir, 1 Langmuir = 10^{-6} torr-sec), the surface density or coverage θ (defined as the ratio of the surface density to the saturation density) can be controlled. The absolute coverage is determined by the thermal desorption and low energy electron diffraction measurement.[27]

For laser-induced thermal desorption, a Q-Switched Nd:YAG laser is used in our case. It produces 10 ns optical pulses at wavelength $\lambda = 1.064\mu$m. The output pulse with an appropriate energy is split into two with intensities I_1 and I_2, respectively. The two pulses are brought to the sample surface at the incident angle $\Phi_{\rm inc}$ from two *different* sides of the surface normal. This produces an intensity pattern at the sample surface with a periodicity

$$2a = \frac{\lambda}{2\sin\Phi_{\rm inc}} \tag{1}$$

The energy absorbed by the substrate heats up the surface region and thus creates a temperature grating. The thermal desorption of the adsorbates by the temperature grating leads to a surface density grating. The desorption rate of adsorbates is usually described by $d\theta/dt = -\nu\theta^n \exp(-\mathbf{E}_{\rm des}/RT)$.[28] n is the pre-exponential factor, n is the desorption order, $\mathbf{E}_{\rm des}$ is the desorption activation energy (in kcal/mol). They are known as the desorption kinetics parameters and are determined by extensive thermal desorption measurements. R is the Boltzman constant in kcal/mole·Kelvin, and T is the sample temperature. Knowing the kinetics parameters and the thermal constants of the substrate, the desorption yield and in turn the remaining adsorbate density can be determined to a high accuracy.[28,29] In practice, the remaining surface density as a function of the heating laser intensity can be obtained experimentally by using an optical second-harmonic micro-probe.[30] From the calibration, one can choose I_1 and I_2 to produce a prescribed surface density grating. In Fig. 2, I show the coverage change $\Delta\theta$ for CO on Ni(111) versus the absorbed laser fluence.

Experimentally, I_1 and I_2 may be set by a properly chosen beam splitter. It is sometimes more desirable to use a 50-50 beam splitter and to use a polarization rotating device (e.g., a half-wave plate) on one arm so that the

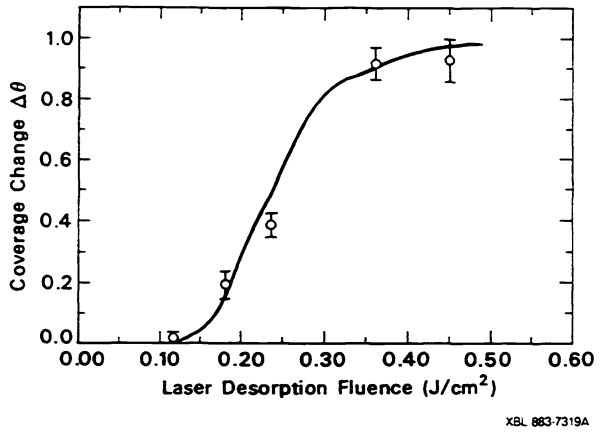

Fig.2. The coverage change of CO on Ni(111) $\Delta\theta$ versus the absorbed laser fluence in a laser-induced thermal desorption measurement. $\Delta\theta$ is deduced from the change of a calibrated, in-situ optical second-harmonic generation. The solid line is calculated from the desorption kinetics parameters.[30]

polarization of the arm can be set continuously from being orthogonal to being parallel to that of the other arm. If the angle of polarization rotation from the parallel position is α, the intensity of the interfering optical field at the sample surface is given by

$$I(x) = I_1 + I_2 + 2\sqrt{I_1 I_2}\cos\alpha\cos(\pi x/a). \tag{2}$$

In this way, we can choose the sum of I_1 and I_2 to yield a prescribed average coverage θ_0, and the polarization angle α to produce a desired modulation depth $\Delta\theta$. The laser-induced adsorbate density grating $\theta(x,t)$ can be expanded in the following spatial Fourier series,

$$\theta(x,t) = \sum_{n=0} \theta_n(t)\cos(n\pi x/a). \tag{3}$$

The time dependence arises from the diffusion of adsorbates. At low enough temperatures, one can characterize the grating with optical diffractions before the effect of the diffusion sets in. In Fig. 3, I show a grating profile of CO on Ni(111) near the center of a laser pulse pair calculated from the calibration curve in Fig. 2. The profile was confirmed by the optical second-harmonic diffraction measurement which is described next.

3. DETECTION OF A MONOLAYER ADSORBATE DENSITY GRATING BY OPTICAL DIFFRACTIONS:

The general consideration of linear and nonlinear optical diffractions from a monolayer adsorbate density grating is same.[22–24,31,32] When a probe laser beam with an electric field $\mathbf{E}_{\rm inc}(\omega)\exp[i(\mathbf{k}_1\mathbf{r}-\omega t)]$ is incident on a substrate covered with adsorbates, the linear and second-order nonlinear optical responses of the surface layer can be characterized by a dipole sheet oscillating at ω, $\mathbf{P}_s(\omega) = \chi^{(1)}(\omega)\mathbf{E}_{\rm inc}(\omega)$ and one oscillating at 2ω, $\mathbf{P}_s(2\omega) = \chi^{(2)}(2\omega)\mathbf{E}_{\rm inc}(\omega)\mathbf{E}_{\rm inc}(\omega)$. If the adsorbate density is modulated, the optical responses are also modulated. If the effect of adsorbate-adsorbate interactions is negligible, we expect $\mathbf{P}_s(\omega)$ and $\mathbf{P}_s(2\omega)$ to be directly proportional to the surface density $\theta(x,t)$,

$$\mathbf{P}_s(\omega) = \mathbf{P}_{s,0}(\omega)\theta(x,t), \tag{4}$$

$$\mathbf{P}_s(2\omega) = \mathbf{P}_{s,0}(2\omega)\theta(x,t). \tag{5}$$

The radiation at either ω or 2ω from an oscillating dipole sheet can be obtained by solving Maxwell equations or directly summing up the radiation from all the oscillating dipoles . For a modulated dipole sheet, one calculates the

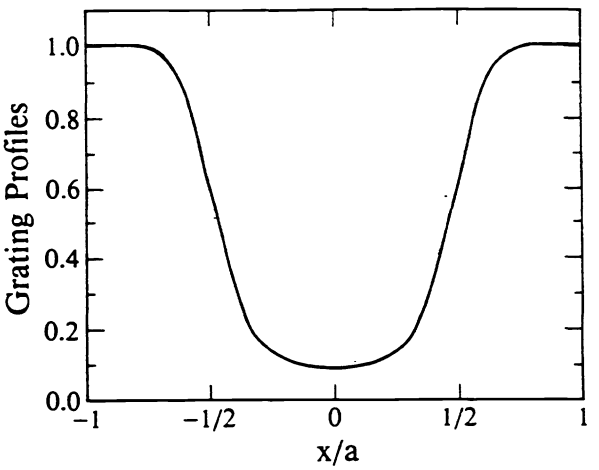

Fig.3. A calculated grating profile of a monolayer grating of CO on Ni(111) within one spatial period $2a$ using the calibration shown in Fig. 2.[22]

radiation corresponding to each spatial Fourier component of Eq. (4) or (5) separately.[22–24] For example, the n-th order diffraction of p-polarization in reflection is given by

$$E_{p,n} = \frac{i2\pi k_1}{\varepsilon_1 k_{1z}}[k_{1z}L_{xx}P_{s,0x} + k_{1x}L_{zz}P_{s,0z}]\frac{\theta_n(t)}{2}, \tag{6}$$

here L_{xx}, L_{yy}, and L_{zz} are the macroscopic local field factors due to the difference of dielectric constants of the monolayer ε', the incidence medium ε_1, and the transmission medium ε_2.[31] $\mathbf{k}_1$ is the magnitude of the wave vector $\mathbf{k}_1$ in medium ε_1, k_{1x} and k_{1z} are components of $\mathbf{k}_1$. The output signal in reflection in photon per second is given by

$$S_{p(s),n} = \frac{c\sqrt{\varepsilon_1}}{2\pi}|E_{p(s),n}|^2\left(\frac{2\pi A}{\hbar\omega}\right)(f\tau). \tag{7}$$

A is the area of the dipole sheet normal to the diffraction direction. f is the repetition rate of a probe laser, and τ is its pulsewidth. For a continuous wave laser, $f\tau$ is taken as unity. The direction of the n-th order diffraction is determined by the usual requirement on the tangential component $k_{n,x}$ of the diffracted radiation wave vector $\mathbf{k}_n$,

$$k_{n,x}(\omega) = k_{1x}(\omega) \pm \frac{n\pi}{a} \tag{8}$$

$$k_{n,x}(2\omega) = 2k_{1x}(\omega) \pm \frac{n\pi}{a} \tag{9}$$

for linear and second-harmonic diffractions, respectively.

I now estimate typical signal strengths for both linear and second- harmonic diffractions. For linear optical diffractions, the signal strengths without local field factor correction can be expressed approximately as

$$S_{p,n}(\omega) = S_{\text{inc}}(\omega)\frac{64\pi^4}{\lambda^2}|N_s\alpha^{(1)}(\omega)|^2\left(\frac{\theta_n}{2}\right)^2. \tag{10}$$

For $N_s\alpha^{(1)}(\omega) \sim 5\times10^{-9} esu, \theta_n \sim 0.4, \lambda \sim 5\times10^{-5}$ cm, $S_{p,n}(\omega) \sim 2\times10^{-6}S_{inc}(\omega)$. Including the local field factor may reduce the signal strengths into 10^{-7} range. For optical second-harmonic diffractions, the signal strengths

without local field factor correction are given similarly by

$$S_{p,n}(2\omega) = S_{inc}(\omega)\frac{64\pi^4}{\lambda^2}|N_s\alpha^{(2)}(2\omega)E_{inc}(\omega)|^2\left(\frac{\theta_n}{2}\right)^2. \quad (11)$$

For a 10 ns laser pulse, a typical peak intensity limited by optical damages for metal substrates is 10 MW/cm^2. This corresponds to $E_{\rm inc}(\omega) \sim 10^2 esu$. For $N_s\alpha^{(2)}(2\omega) \sim 10^{-15} esu$, we have $N_s\alpha^{(2)}(2\omega)E_{inc}(\omega) \sim 10^{-13} esu$. Thus for $\theta_n \sim 0.4, \lambda \sim 5 \times 10^{-5}$ cm, $S_{p,n}(2\omega) \sim 10^{-15} S_{inc}(\omega)$.

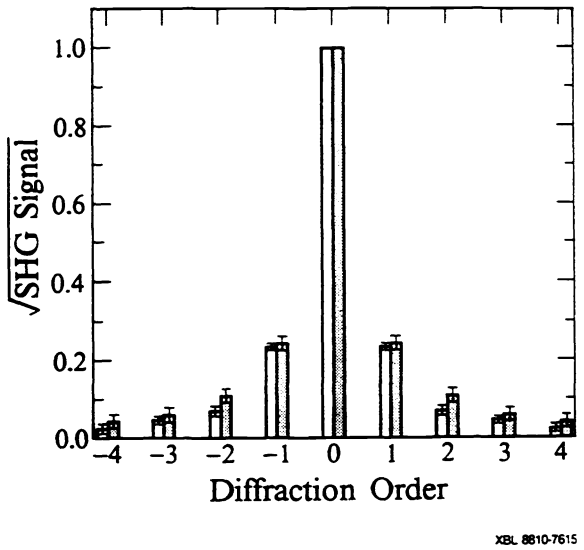

Fig.4. The square roots of optical second-harmonic diffractions $[S_n(2\omega)]^{1/2}$ from a monolayer grating of CO on Ni(111) as shown in Fig. 3.[22] Unshaded columns: measured signals. Shaded columns: calculated signals from the results of Fig. 3.

In Fig. 4, I show the optical second-harmonic radiation fields from a density grating of CO on Ni(111).[22] The shaded columns are calculated from the profile in Fig. 3. The agreement is very well. In Fig. 5, I show the linear optical diffractions of a He-Ne laser beam from a grating of a monolayer Rhodamine 6G molecules on fused silica. It should be noted that the linear diffractions are not resonance- enhanced at the He-Ne laser wavelength.

It is clear that the strengths of linear diffractions are 10^8 times of second-harmonic diffractions for same averaged probe beam powers. It is thus necessary to comment on the usefulness of nonlinear optical diffractions. It is known that linear optical diffractions are accompanied by a diffuse scattering background from the residual roughness on a nominally flat substrate.[22,24] The unwanted background is the regular bulk reflection from optically rough regions. As a linear bulk reflection is 10^6 times as intense as that from a monolayer, an optically rough region of 10^{-6} of the total illuminated surface area is sufficient to yield a background light which overwhelms linear optical diffractions from monolayer gratings. Special cares thus must be taken to eliminate the background contribution.[32]

This problem is lifted by symmetry in optical second-harmonic diffractions.[22] Although being a much weaker optical process, the diffuse scattering from the bulk at the second-harmonic frequency is dramatically suppressed when substrates have centers of inversion or an isotropic order.[33,34] The residual diffuse second-harmonic scattering comes mainly from much weaker electric quadrupole and magnetic dipole responses of the bulk.[35] Consequently, the ratio of second-harmonic diffractions from monolayer adsorbate gratings to the diffuse second-harmonic background is enhanced by a factor of 104 to 106 from that of a linear optical diffraction. This has enabled Reider et al, Zhu et al, and Suzuki et al to observe the optical second-harmonic diffractions from monolayer adsorbate gratings to high orders.

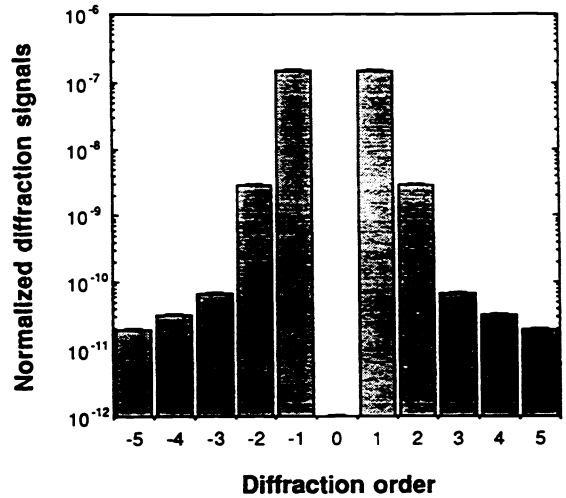

Fig.5. The measured linear optical diffraction signals from a monolayer grating of Rhodamine 6G molecules on a fused silica. All signals are normalized to the strength of an incident He-Ne laser beam.[24]

The only disadvantage of optical second-harmonic diffractions is the weakness of its absolute strength. Limited by optical damages, first-order optical second-harmonic diffractions from a fully modulated monolayer adsorbate density grating with an area of 10 mm^2 are typically 0.05 - 0.2 photon-counts per laser pulse.[16,18] For modulations less than 10% of one monolayer, diffraction signals decrease quickly to a prohibitively low level. This makes a coverage dependence investigation very difficult.

Generally speaking, for substrate systems which exhibit large changes in surface nonlinear optical responses upon adsorption of adsorbates such as hydrogen on Si(111) and CO on Ni(111), optical second-harmonic diffractions are justified as good probes to surface density gratings. Otherwise, linear optical diffractions are better choices.

4. EVOLUTION OF A MONOLAYER ADSORBATE DENSITY GRATING AND THE MEASUREMENT OF SURFACE DIFFUSION COEFFICIENTS:

At a finite temperature T, an adsorbate density grating evolves in time according to the Fick's law. Since the overall size of a laser- induced grating is usually much larger than the grating periodicity, we have at hand a one dimensional diffusion problem,

$$\frac{\partial \theta}{\partial t} = \frac{\partial}{\partial x}\left[D(\theta)\frac{\partial \theta}{\partial x}\right]. \tag{12}$$

The one dimensionality is characterized by aspect ratios of 10^3 to 10^4. $D(\theta)$ is the chemical diffusion coefficient which includes the effect of adsorbate-adsorbate interactions after an appropriate thermodynamic average. It should be distinguished from a tracer diffusion coefficient which is obtained at the zero coverage. When the interaction is of short range and thus acts only to block the available destiny sites for a moving adsorbate or when the measurement is performed at low coverages, the chemical diffusion coefficient is expected to approach the tracer diffusion coefficient. Such an approximation is useful as most microscopic theories of diffusion coefficients are established in the zero coverage limit.

When the coverage dependence of the diffusion coefficient $D(\theta)$ is weak for a given coverage modulation $\Delta\theta$, we can approximate Eq. (12) by replacing $D(\theta)$ with $D(\theta_0)$. The n-th spatial Fourier component of the adsorbate

density grating $\theta_n(t)$ is easily obtained,

$$\theta_n(t) = \theta_n(0)\exp[-n^2\pi^2 D(\theta_0)t/a^2]. \tag{13}$$

And we find that optical diffraction signals evolves as

$$S_n(t) = S_n(0)\exp[-2\pi^2 n^2 D(\theta_0)t/a^2]. \tag{14}$$

One extracts $D(\theta_0)$ from the measured exponents.

Optical diffraction techniques are capable of measuring diffusion coefficients in a large dynamic range. From Eq. (14), the range of measurable diffusion coefficients is determined by $D \sim a^2/2\pi^2 n^2 t$. Typically, t varies from 10 to 10^4 sec which is determined by signal-to- noise ratios and contaminations in a 10^{-10} to 10^{-11} torr vacuum. With a $\sim 10^{-2}$ to 10^{-5} cm, we arrive at a range of measurable D from 5×10^{-7} cm^2/sec to 5×10^{-16} cm^2/sec, if the first order diffraction is measured. The lower limit may be extended further when higher order diffractions are employed. Few techniques match optical diffraction techniques in this regard.[1] It has made it possible for us to study the quantum tunneling diffusion of hydrogen which has rates below 10^{-10} cm^2/sec.[2,3,5,21]

5. EXAMPLES OF OPTICAL DIFFRACTION STUDIES OF ADSORBATE DIFFUSION:

There have been numerous reports of surface diffusion measurements by using optical diffractions from surface density gratings. Early works by Maiya, Blakely, Bonzel and Yamashita et al involved photolytically etched periodic profiles on single crystal metals.[36–39] These profiles are tens of microns wide and a fraction of a micron deep. In these studies, steps of high densities and facets may have affected the diffusion either directly or indirectly through altering the properties of the terraces. Recently, Zhu et al [CO on Ni(111)] and Reider et al [H on Si(111)] successfully performed the measurements of surface diffusion coefficients by using optical second-harmonic diffractions.[16,17] Xiao et al studied anisotropic diffusion of CO on Ni(110).[18] More recently, we applied linear optical diffractions to the studies of hydrogen and deuterium on Ni(100) and Ni(111) down to 108 K and observed the onset of quantum tunneling.[21,25]

a. Measurements of slow over-barrier diffusions: CO on Ni(111)

In a macroscopic diffusion measurement, one usually observes the evolution of a density profile with a probe over a length scale L. It is determined by either the formation of the density profile or by the probe. This sets a lower limit of measurable diffusion coefficient $D_{\min}$ if an upper limit of the measurement time $t_{\max}$ exists so that $D_{\min} \sim L^2/t_{\max}$. The proportionality constant is typically 0.1. For adsorbate diffusion on a single crystal in an ultrahigh vacuum, $t_{\max}$ is the time beyond which the re-adsorption from an ambient becomes unacceptable. At an operating base pressure of 1×10^{-10} torr, $t_{\max}$ is 10^4 sec which is roughly the time to cover a clean surface with a full monolayer of "impurity adsorbates". For the laser-induced hole-burning mass spectrometry technique of George et al, the length scale is limited by the spot size of a heat laser beam to 300 μm so that $D_{\min} \sim 1 \times 10^{-9}$ cm^2/sec.[40] For a Field emission microscope used by Gomer and coworkers, the length scale L is about 500 Åand is determined by the metal emission tip. The minimum measurable diffusion coefficient is nominally $D_{\min} \sim 2 \times 10^{-16}$ cm^2/sec. Optical diffraction techniques are also capable of detecting as small a diffusion coefficient as 10^{-16} cm^2/sec.

The study of CO on Ni(111) is the first case of using optical diffractions from laser-induced monolayer density gratings in a surface diffusion measurement.[16] CO on Ni(111) also represents a case of slow diffusion.

In Fig. 6, I reproduce the first order optical second- harmonic diffractions from monolayer gratings of CO on Ni(111) versus the observation time. The measurements were carried out from 220 K to 270 K. The grating spacing $2a$ was chosen to be 20 μm. The decay of the diffraction signal is fit to a single exponential function. The diffusion

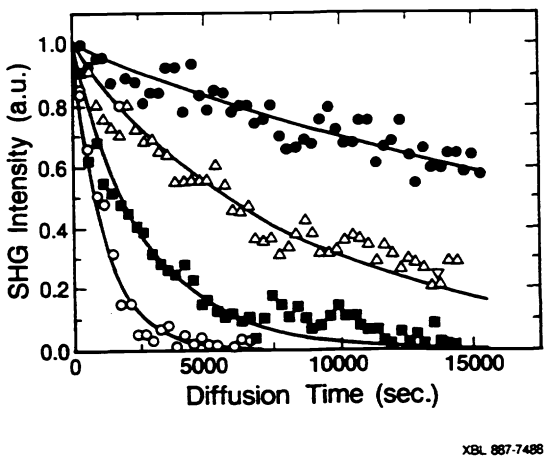

Fig.6. Normalized first-order optical second-harmonic diffraction signals from monolayer gratings of CO on Ni(111) vs the observation time. Solid circles: T = 219 K; open triangles: T = 247 K; solid squares: T = 261 K; open circles: T = 273 K. The solid curves are least-square fits using single exponential functions.

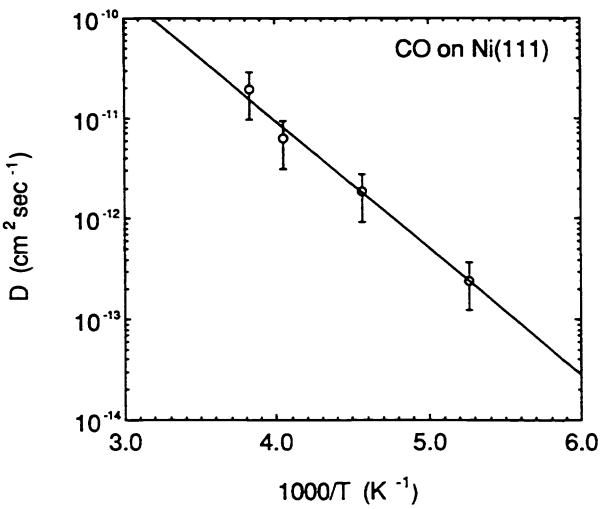

Fig.7. Arrehnius plot (open circles) of the diffusion coefficients D(T) of CO on Ni(111) from 219 K to 273 K obtained from the results shown in Fig. 6

coefficients $D(T)$ are obtained from the exponents using Eq. (14). To display the temperature dependence, D(T) is plotted in the Arrehnius form in Fig. 7. It is fit well with a functional form of $D(T) = D_0 \exp(-E_{\text{diff}}/RT)$. The diffusion activation energy E_{diff} is determined to be 7 kcal/mol, and the diffusivity $D_0 = 1.2 \times 10^{-5}$ cm^2/sec. It is attributed to an over-barrier hopping of CO from a bridge site over a terminal site and to a neighboring bridge site. It should be noted that if the grating spacing was taken to be 1 mm, the diffusion would be noticeable only at 700 K over 10^4 seconds. By then the adsorbed CO would have been long gone.

Another example of slow diffusion is that of chemisorbed hydrogen on Si(111).[17] It was recently investigated by Reider et al with the optical second-harmonic diffractions from laser-induced hydrogen density gratings. The authors had to use grating spacings of a fractional micron in order to curtail the thermal desorption effect.

b. Study of anisotropy of surface diffusion: CO on Ni(110)

A strong feature of optical diffraction techniques is the capability to resolve the anisotropy of a surface diffusion with a high aspect ratio. Xiao et al. studied the anisotropy of the diffusion of CO on Ni(110) by rotating the grating with respect to a surface crystalline axis and measuring the diffusion coefficient at various azimuthal angles.[18] The diffusion coefficient $D(T)$ is reproduced in Fig. 8. The authors were able to identify two distinct diffusion channels, one along [110] direction with $E_{\text{diff}} = 1.1$ kcal/mol and $D_0 = 3.8 \times 10^{-9}$ cm^2/sec and the other along [100] with $E_{\text{diff}} = 3.1$ kcal/mol and $D_0 = 4.8 \times 10^{-6}$ cm^2/sec. This is experimentally significant since there does not exist a priori knowledge on what the surface potential distribution is or should be like for CO on Ni(110) or on any other surfaces. The activation energy along [110] axis, $\sim$ 1 kcal/mol, is rather small. Adsorbate-adsorbate interactions and the presence of impurities can easily lift the preference of specific sites on the ridges of [110] Ni atom rows. This observation is consistent with the reports of rich superlattice structures of overlayer CO at different coverages, particularly the molecular arrangements along [110] rows.

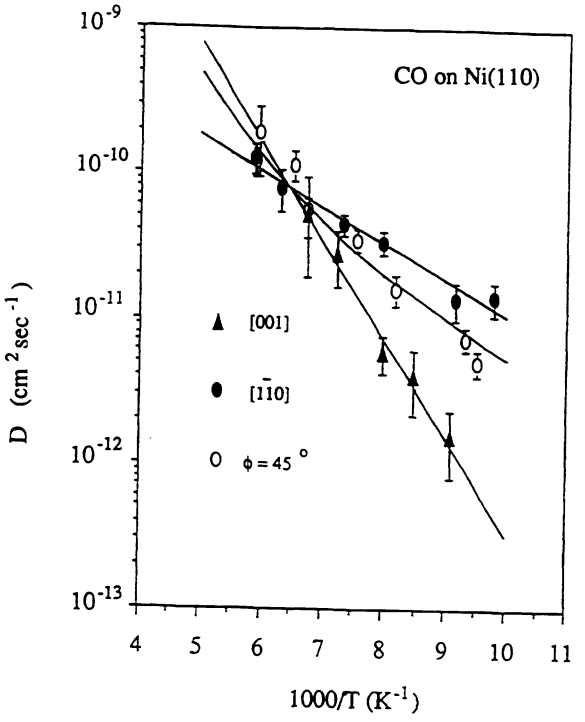

Fig.8. Arrehnius plots of the diffusion coefficients $D(T, \phi)$ for CO on Ni(110). ϕ is the azimuthal angle between the [110] axis of the Ni substrate and the orientation of the CO coverage grating. Solid triangles: $\phi = 0°$. Solid circles: $\phi = 90°$. Open circles: $\phi = 45°$.

c. Study of quantum tunneling diffusions: H and D on Ni(100) and Ni(111):

The diffusion of light atoms in solids through under-barrier tunneling is a most actively studied topics in condensed matters physics.[2,3,4,7–13] There are intensive effort to investigate the tunneling under the influences of phonons, conduction electrons, and other low lying excitations in solids. Hydrogen isotopes on metals and semiconductors are ideal candidates for an experimental exploration.[2,3,19,21] The diffusion rate due to quantum tunneling is typically in the range of 10^{-10} to 10^{-14} cm^2/sec. Optical diffraction probes are well suited for experimental

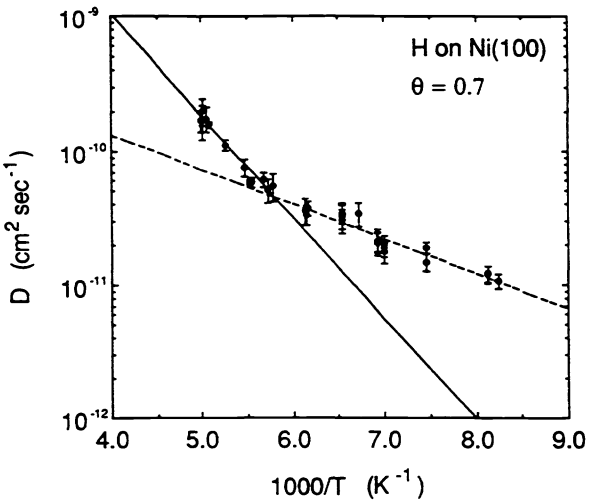

Fig.9. Arrehnius plot of the diffusion coefficient $D(T)$ for hydrogen atoms on Ni(100) at a coverage $\theta = 0.7$. The temperature range is from 120 K to 200 K. The kink in the data occurs at T = 160 K. Solid line: an Arrehnius fit to the high temperature behavior. Dash line: an Arrehnius fit to the low temperature behavior.

investigations. With the high sensitivity of linear diffraction probes, the measurements can be extended to a large number of substrate systems and large ranges of coverages. This makes comprehensive investigations possible.

We have started a systematic study of hydrogen diffusion on metals using a linear optical diffraction method.[21,25] We measured diffusion coefficients for hydrogen and deuterium on Ni(100) and Ni(111) in the temperature range from 200 K to 108 K. In these measurements, the grating half-periods a from 8.3 μm to 4.2 μm are used. The average coverages θ_0 are varied from 0.5 to 0.7. The modulations are less than 10% of one monolayer. The first order diffraction of a 2 mW He-Ne laser is used to probe the evolution of the hydrogen coverage gratings.[19,24] The measured $D(T)$ for hydrogen on Ni(100) is plotted in Fig. 9. The results clearly indicate two thermally activated regions. $D_0 = 1.1 \times 10^{-6}$ cm^2/sec and $E_{\text{diff}} = 3.5$ kcal/mol from 200 K to 160 K, while $D_0 = 1.5 \times 10^{-9}$ cm^2/sec and $E_{\text{diff}} = 1.2$ kcal/mol from 160 K to 120 K. Our results at high temperatures confirm the measurements at even higher temperatures by other groups using the field emission microscope and laser-induced hole-burning mass spectrometry techniques.[3,40] It is attributed to an over-barrier hopping from a four-fold hollow site over a two-fold bridge site to a neighboring hollow site. We attribute the low temperature activated diffusion to an activated tunneling as described by the small-polaron model due to Holstein [8,9]. The activation energy, 1 kcal/mol, correlates well with an estimate of the lattice relaxation energy based upon the available surface phonon data on Ni(100).[21]

In Fig. 10, I display the Arrehnius plot of the measured diffusion coefficient of hydrogen and deuterium on Ni(111) from 108 to 200 K.[25] The mean coverage is $\theta_0 = 0.5$. The temperature dependence is strikingly different. The over-barrier hopping is not followed by a conventional activated tunneling as displayed by hydrogen on Ni(100). As the temperature decreases, the diffusion rate transform from an activated behavior to a small upturn at 125 K before leveling off at around 108 K. This behavior is not easily explained within the frame work of present small-polaron model even when the conduction electron effect and the finite coverage effect are taken into account.[4-12] We have tentatively attributed the behavior to the effect of a quadratic coupling between hydrogen and the underlining Ni(111).[41] As a quadratic coupling does not lead to local lattice relaxation, the finite temperature only spoils the tunneling. This gives rise to a tunneling rate which increases as T decreases.

6. CONCLUDING REMARKS

Optical diffractions from surface density gratings as probes to diffusion of adsorbates are very promising. In the few reported experiments, their most desirable features are shown to be ideally suited for the purpose. We are at the stage when in-depth investigations are possible and practical. We have just started a long- term research on the experimental aspects of quantum tunneling diffusions of light atoms. The goal is to elucidate the mechanisms behind

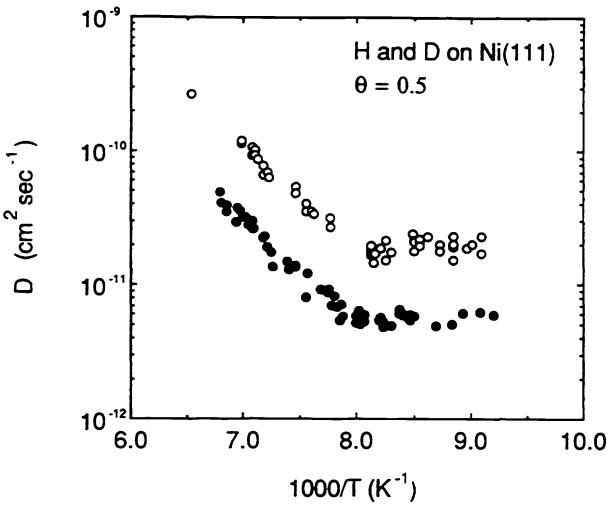

Fig.10. Arrehnius plot of the diffusion coefficient D(T) for H (open circles) and deuterium (solid circles) on Ni(111) at a coverage $\theta = 0.5$.

the dissipative tunneling and the roles of such parameters as phonons, conduction electrons, surface morphology, adsorbate-adsorbate and adsorbate-substrate interactions. In addition, we will see more experimental data obtained by optical diffraction probes over much larger ranges of temperature and other static and kinetic parameters such as coverages, coadsorption, and vicinal surfaces. This will surely improve and further our current understanding of surface diffusion in a more complete and coherent fashion.

7. ACKNOWLEDGEMENT

The author wishes to sincerely thank Professor Y.R. Shen, Th. Rasing, W. Daum, Xudong Xiao, A. Lee, A. Wong, and U. Linke for the collaboration at various stages of the development of the optical diffraction technique. This work has been supported by the Director, Office of Energy Research, Office of Basic Energy Sciences, Materials Sciences Division of the U.S. Department of Energy under Contract No. DE-AC03-76SF00098, by the National Science Foundation under Grant No. DMR-9104109 and in part by American Chemical Society under the Petroleum Research Fund No. 24373G5.

8. REFERENCES

1. Gomer, Rep. Prog. Phys. **53**, 917 (1990).
2. R. DiFoggio and R. Gomer, Phys. Rev. **B 25** , 3490 (1982).
3. T.-S. Lin and R. Gomer, Surf. Sci. **225**, 41 (1991).
4. K. W. Fehr, in Hydrogen in Metals I, eds., G. Alefeld and J. Vlkl (Springer, New York, 1978), Chap. 8, pp. 197-226; J. Vlkl and G. Alefeld, ibid., Chapt. 12, pp. 321-348.
5. V.G. Grebinnik, I.I. Gurevich, V.A. Zhukov, A.P. Manich, E.A. Mel'eshko, I.A. Muratova, B.A. Nikol'skii, V.I. Selivanov, and V.A. Suetin, Zh. Eksp. Teor. Fiz. **68**, 1548 (1975) [Soviet Phys.-JETP **41**, 777 (1975)].
6. H. Teichler, Phys. Lett. **64 A**, 78 (1977).
7. R.K. Kiefl, R. Kadono, J.H. Brewer, G.M. Luke, H.K. Yen, M. Celio, and E.J. Ansaldo, Phys. Rev. Lett. **62**, 792 (1989).
8. T. Holstein, Ann. Phys. **8**, 343 (1959).

9. C.P. Flynn and A.M. Stoneham, Phys. Rev. **B 1**, 3966 (1970).
10. J. Kondo, Physica 84 B, 40 (1976); ibid., **126 B**, 377 (1984); ibid., **125 B**, 279 (1984); ibid., **141 B**, 305 (1986).
11. A.J. Leggett, S. Chakravarty, A.T. Dorsey, M.P.A. Fisher, A. Garg, and W. Zwerger, Rev. Mod. Phys. **59**, 1 (1987).
12. M.I. Klinger, Phys. Rep. **94**, 183 (1983).
13. Q. Niu, J. Stat. Mech. **65**, 317 (1991), and references therein.
14. M.J. Puska, R.M. Nieminen, M. Manninen, B. Chakraborty, S. Holloway, and J.K. Norskov, Phys. Rev. Lett. **51**, 1081 (1983), and references therein.
15. M.J. Puska and R.M. Nieminen, Surf. Sci. **157**, 413 (1985).
16. X.D. Zhu, Th. Rasing, and Y.R. Shen, Phys. Rev. Lett. **61**, 2883 (1988).
17. G.A. Reider, U. Hofer, and T.F. Heinz, Phys. Rev. Lett. **66**, 1994 (1991).
18. Xudong Xiao, X.D. Zhu, W. Daum, and Y.R. Shen, Phys. Rev. Lett. **66**, 2352 (1991).
19. X.D. Zhu, A. Lee, A. Wong, and U. Linke, Phys. Rev. Lett. **68**, 1862 (1992).
20. Xudong Xiao, X.D. Zhu, W. Daum, and Y.R. Shen, Phys. Rev. **B 46**, 9732 (1992).
21. A. Lee, X.D. Zhu, L. Deng ,and U. Linke, Phys. Rev. **B 46**, 15472 (1992).
22. X.D. Zhu and Y.R. Shen, Opt. Lett. **14**, 503 (1989).
23. T. Suzuki and T.F. Heinz, Opt. Lett. **124**, 1201 (1989).
24. X.D. Zhu, A. Lee, and A. Wong, Appl. Phys. **A 52**, 317 (1991) and references therein.
25. A. Lee, A. Wong, X.D. Zhu, and U. Linke, to be submitted.
26. H.J. Eichler, P. Gunter, and D.W. Pohl, Laser-Induced Dynamic Gratings (Springer, Berlin and Heidelberg, 1986).
27. G.A. Somorjai, Chemistry in Two Dimensions: Surfaces (Cornell University Press, Ithaca, New York, 1981).
28. P.A. Redhead, Vacuum **123**, 203 (1962); D.A. King, Surf. Sci. **47**, 384 (1975).
29. J.H. Bechtel, J. Appl. Phys. **46**, 1585 (1975).
30. X.D. Zhu, Th. Rasing, and Y.R. Shen, Chem. Phys. Lett. **155**, 459 (1989).
31. Y.R. Shen, Ann. Rev. Phys. Chem. **40**, 327 (1989).
32. J.D. McIntyre and D.E. Aspnes, Surf. Sci. **24**, 417 (1971).
33. T.F. Heinz, C.K. Chen, D. Ricard, and Y.R. Shen, Phys. Rev. Lett. **46**, 1010 (1981).
34. Y.R. Shen, The Principles of Nonlinear Optics (Wiley, New York, 1984), p. 494; Ann. Rev. Mater. Sci. **16**, 69 (1986).
35. P. Guyot-Sionnest and Y.R. Shen, Phys. Rev. **B 33**, 8254 (1986).
36. J.M. Blakely and M. Mykura, Acta Metall. **10**, 565 (1962).
37. H.P. Bonzel and E.E. Latta, Surf. Sci. **76**, 275 (1978).
38. P.S. Maiya and J.M. Blakely, J. Appl. Phys. **38**, 698 (1967).
39. K. Yamashita, H.P. Bonzel, and H. Ibach, Appl. Phys. **25**, 231 (1981).
40. S. M. George, A. M. DeSantolo, and R. B. Hall, Surf. Sci. **159**, L425 (1985).
41. L. Deng and X. D Zhu, submitted to Phys. Rev. Lett.